Supporting Information

Reconfigurable Manipulation of Oxygen Content on Metal Oxide Surfaces and Applications to Gas Sensing

*Gyuweon Jung[1], Suyeon Ju[2], Kangwook Choi[1], Jaehyeon Kim[1], Seongbin Hong[1], Jinwoo Park[1], Wonjun Shin[1], Yujeong Jeong[1], Seungwu Han[2], Woo Young Choi[1], and Jong-Ho Lee[1,3]**

[1]*Department of Electrical and Computer Engineering and Inter-university Semiconductor Research Center, Seoul National University, Seoul 08826, Republic of Korea*

[2]*Department of Materials Science and Engineering and Research Institute of Advanced Materials, Seoul National University, Seoul 08826, Republic of Korea*

[3] *Ministry of Science and ICT, Sejong 30121, Republic of Korea*

* Corresponding author. Tel.: +82-2-880-1727; Fax: +82-2-882-4658.

E-mail address: jhl@snu.ac.kr (J.-H. Lee)

CONTENTS

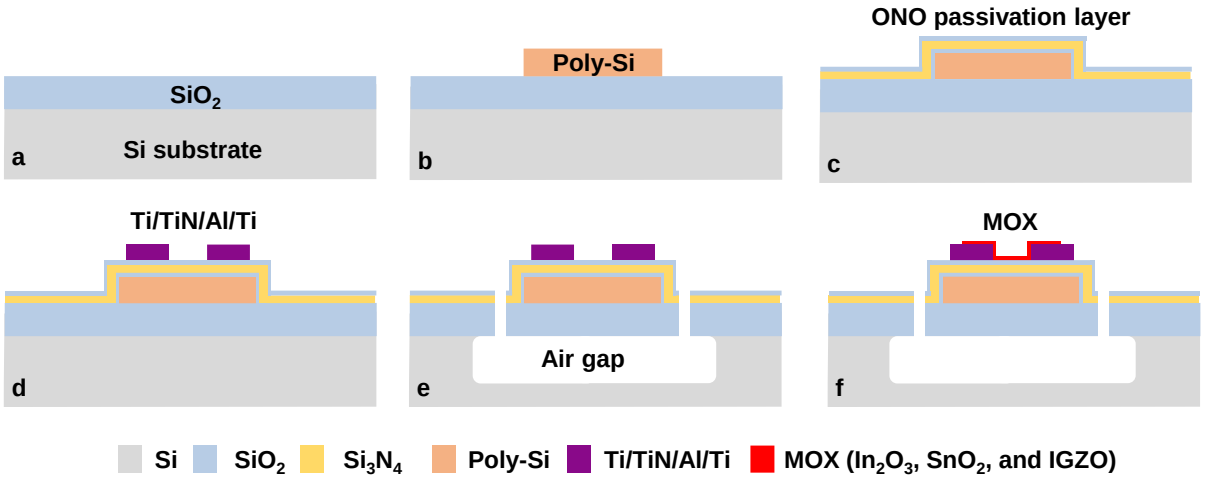

Figure S1. Fabrication processes of MOX devices. (a) 350 nm thick silicon oxide is thermally grown through wet oxidation. (b) n^+-doped polysilicon is deposited and patterned to form microheaters (gates). (**c**) Deposition of the passivation layer of $SiO_2/Si_3N_4/SiO_2$ (10 nm/20 nm/10 nm) to prevent contamination. (d) Metal line (Ti/TiN/Al/TiN (20 nm/20 nm/70 nm/20 nm)) formation after defining the contact holes. (e) Formation of an air gap to prevent heat loss. (f) Deposition and patterning of the MOX layer (In_2O_3, SnO_2, and IGZO).

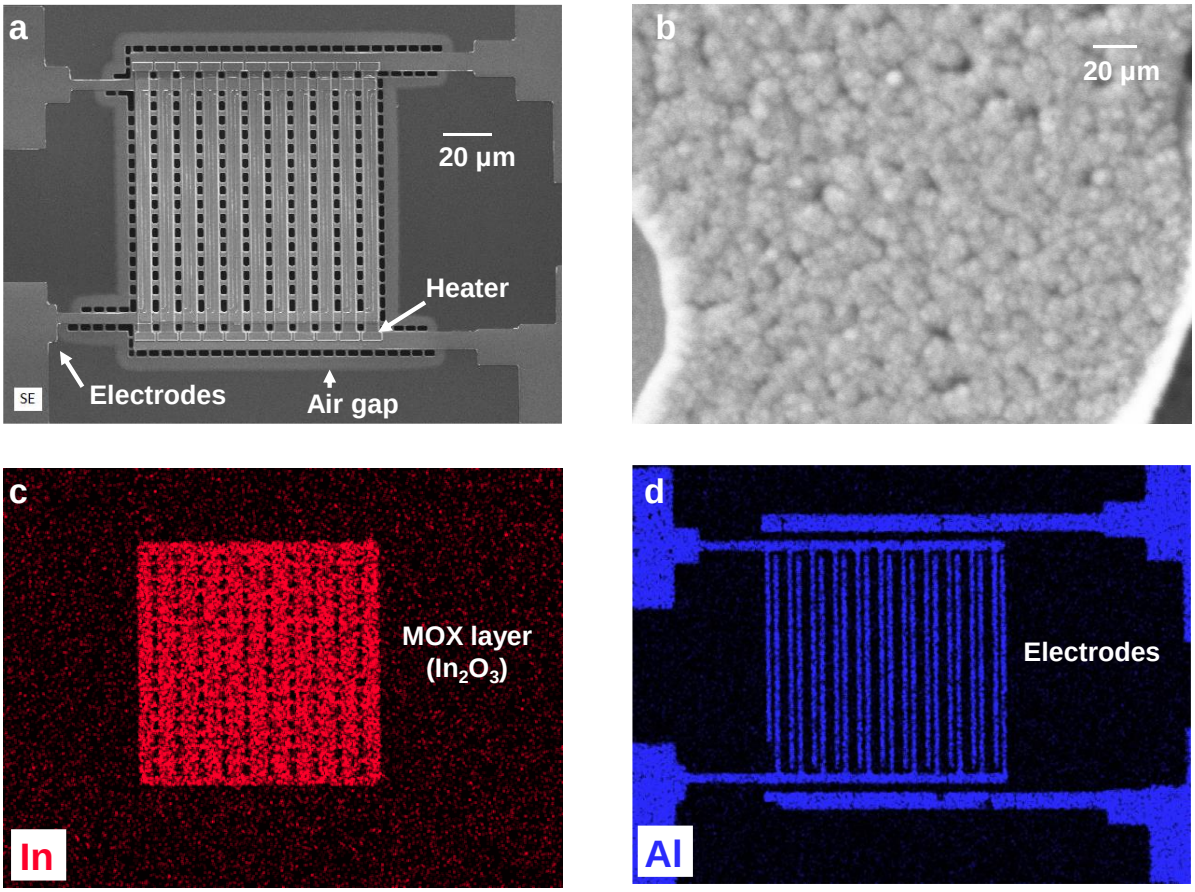

Figure S2. Scanning electron microscopy (SEM) images and energy-dispersive X-ray spectroscopy (EDS) mapping images of the fabricated device with In_2O_3. (a) Top SEM image of the fabricated resistive SMOX gas sensor with a microheater. (b) Top SEM image of In_2O_3. EDS mapping images of (c) indium and (d) aluminum.

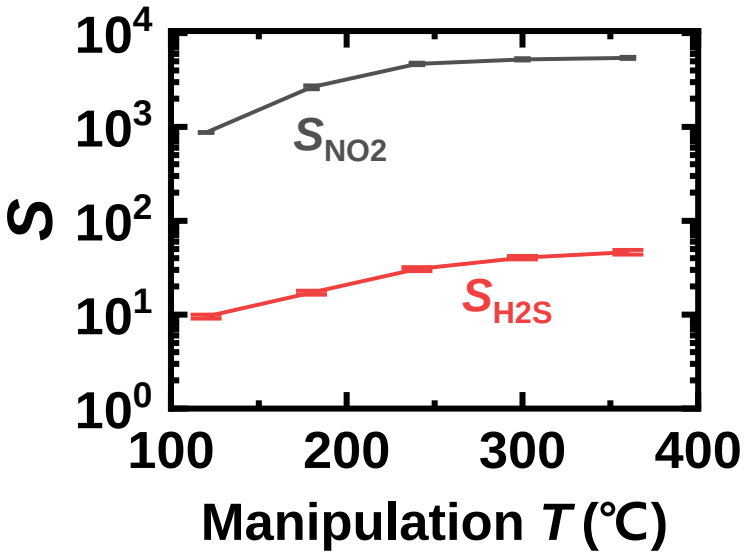

Figure S3. Response characteristics of an In_2O_3 gas sensor to 500 ppb NO_2 gas and 50 ppm H_2S gas as a function of oxygen manipulation temperature.

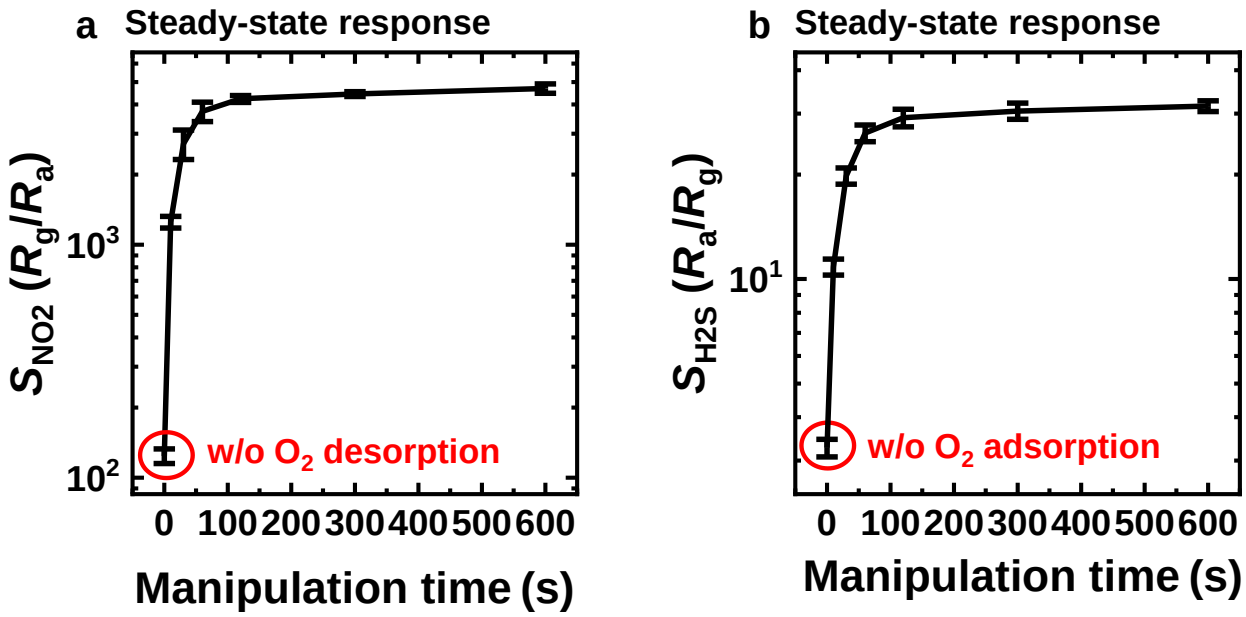

Figure S4. Response characteristics of an In_2O_3 gas sensor to 500 ppb NO_2 gas (a) and 50 ppm H_2S gas (b) as a function of oxygen manipulation time at 240 °C.

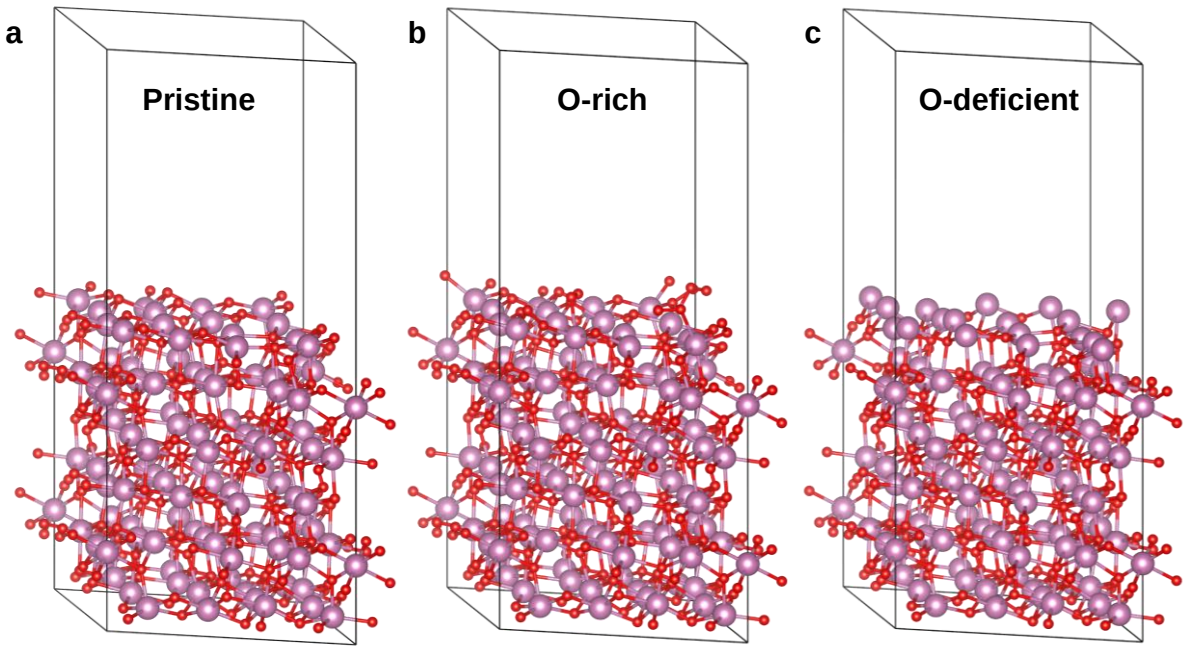

Figure S5. Various In_2O_3 slabs used for DFT calculations. (a) Pristine, (b) O-rich, and (c) O-deficient indium oxide structures.

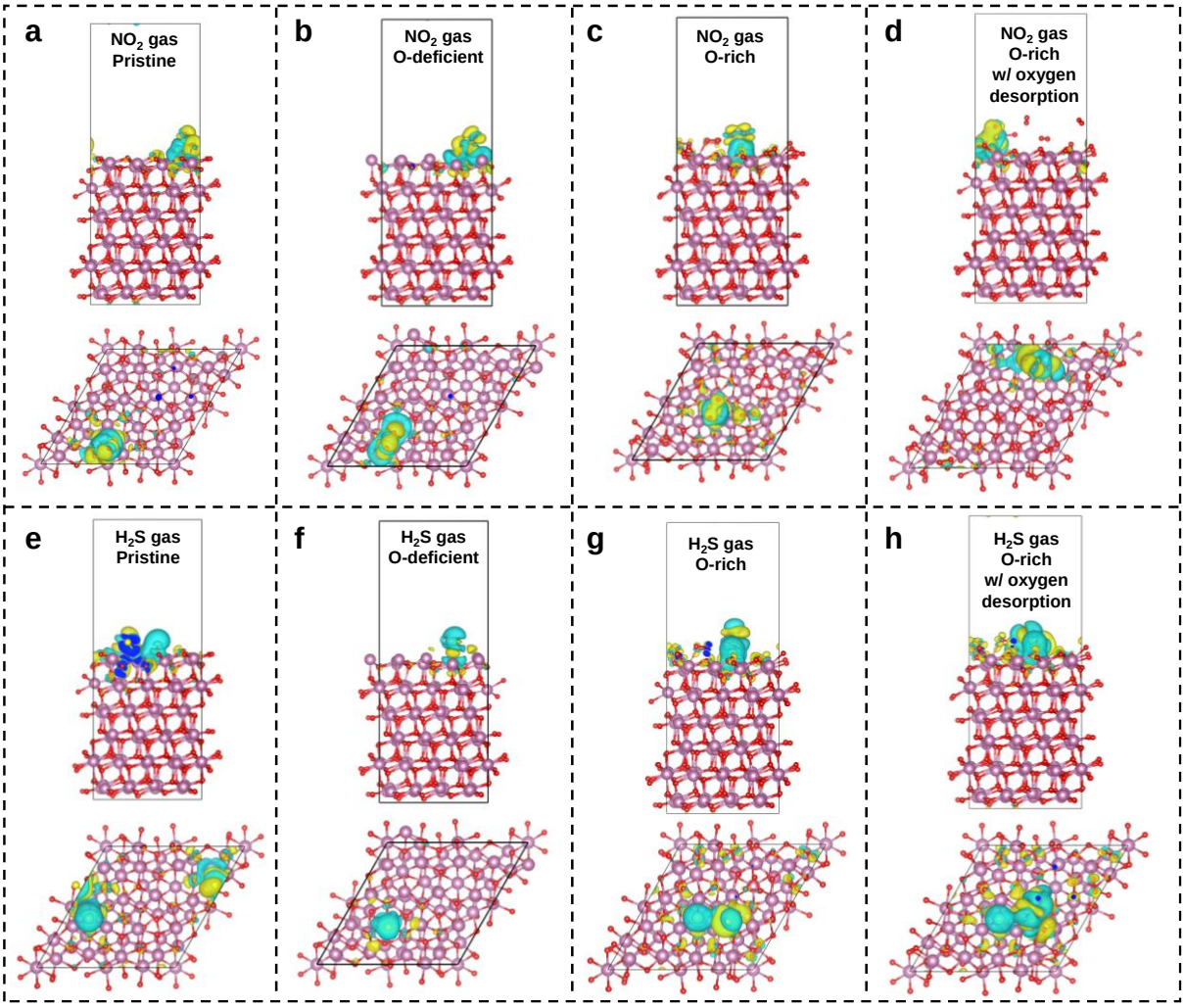

Figure S6. Bader charge analyses of NO_2 and H_2S gas adsorption on the In_2O_3 (111) surface. Bader charge difference plots of (a)–(d) NO_2 gas and (e)–(h) H_2S gas adsorption on pristine (a, e), O-deficient (b, f), and O-rich (c, d, g, h) In_2O_3 surfaces. The blue and yellow charge distributions represent the positive and negative electron density changes after gas adsorption, respectively.

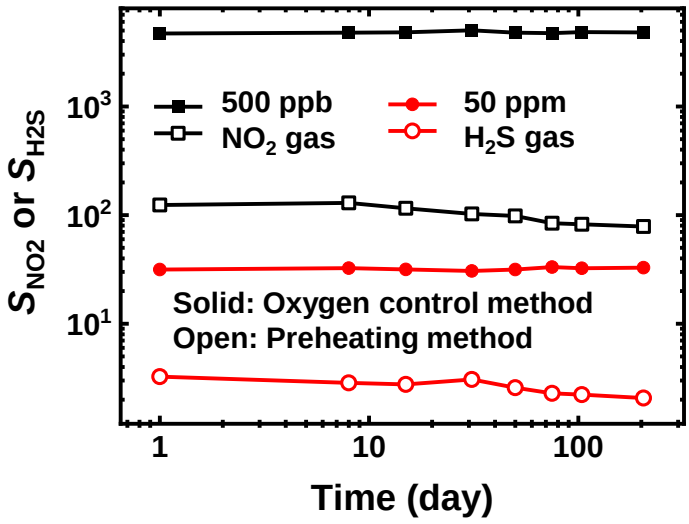

Figure S7. Steady-state response of the sensor to 500 ppb NO_2 and 50 ppm H_2S gas over time using the conventional preheating method and the proposed oxygen control method.

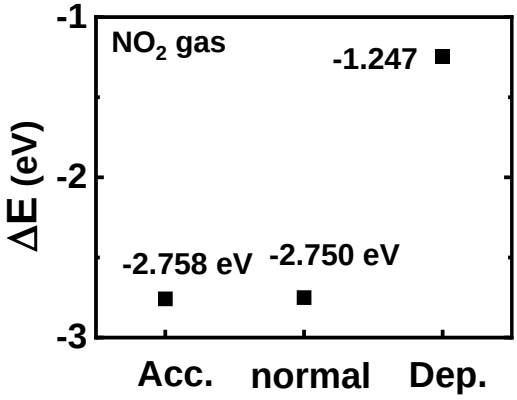

Figure S8. Binding energy (ΔE) values of NO_2 at different In_2O_3 electron concentrations.

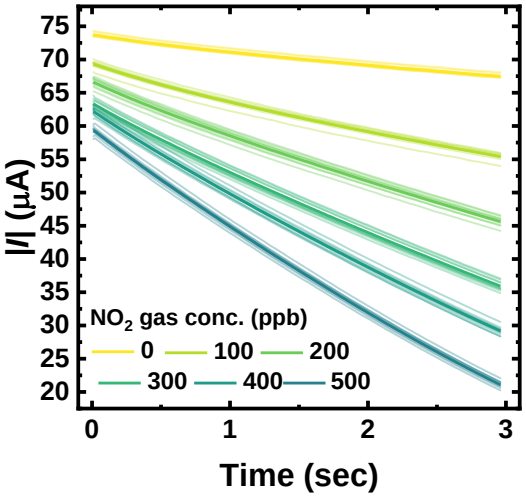

Figure S9. Transient responses of the sensors to 0–500 ppb NO_2 gas obtained after using the gas desorption method. Ten transient responses from each of the six gas concentrations and their average values are shown as transparent and solid lines, respectively.

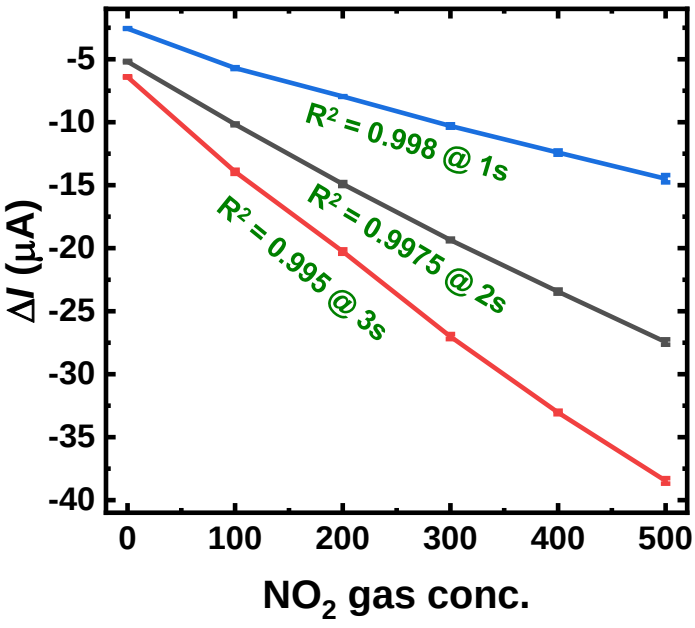

Figure S10. ΔI versus NO_2 gas concentration. The mean and one standard deviation of 10 ΔI are plotted using error bars.

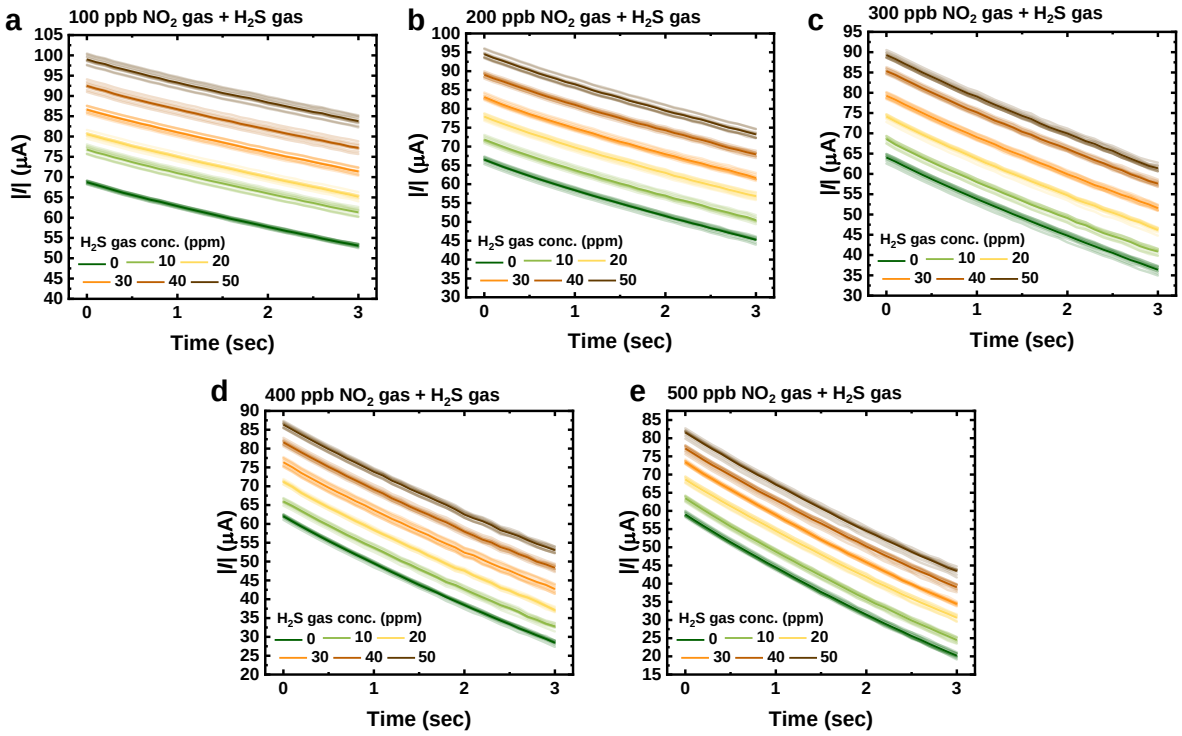

Figure S11. Transient sensor responses to NO_2 and H_2S gas mixtures after oxygen desorption. (a)-(e) The sensor is exposed to a combination of 100–500 ppb NO_2 gas and 10–50 ppm H_2S gas. Ten transient responses from each of the six gas concentrations and their average values are shown as transparent and solid lines, respectively.

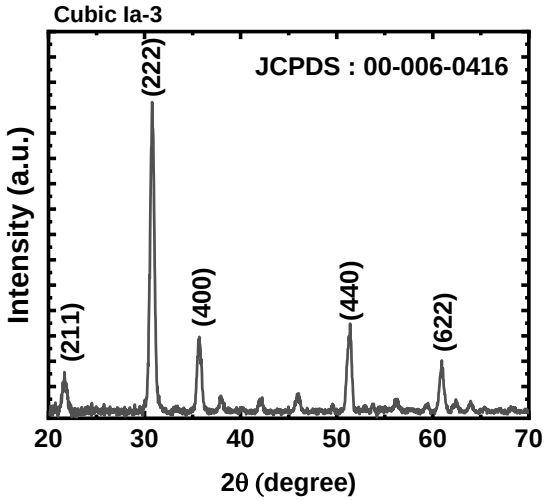

Figure S12. GIXRD pattern of 18 nm In_2O_3 film.

Table S1. Area ratio of the bands fitted to the O_{1s} XPS peak from the indium oxide film.

	O-In (%)	Others (%)
Pristine	49.7	50.3
O-deficient	47.9	52.1
O-rich	53.8	46.2

Table S2. Area ratio of the bands fitted to the In_{3d} XPS peak.

	O-In (%)	Others (%)
Pristine	79.2	20.8
O-deficient	73.4	26.6
O-rich	81.8	18.2

Table S3. Bader charge analyses of NO_2 gas adsorption on the In_2O_3 (111) surface.

	Surface	N	O	O
Pristine	0.034	0.827	-0.500	-0.361
O-deficient	0.614	0.397	-0.580	-0.432
O-rich (w/ oxygen desorption)	0.157	0.862	-0.622	-0.396
O-rich (w/o oxygen desorption)	-0.110	0.854	-0.385	-0.359

Table S4. Bader charge analyses of H_2S gas adsorption on the In_2O_3 (111) surface.

	Surface	S	H	H
Pristine	-0.172	-0.450	0.035	0.587
O-deficient	-0.054	-0.097	0.066	0.085
O-rich (w/ oxygen desorption)	-2.347	1.651	0.093	0.603
O-rich (w/o oxygen desorption)	-1.277	0.605	0.058	0.614